Res Chem Intermed (2016) 42:3789–3804
DOI 10.1007/s11164-015-2245-5

meso-Aryl-substituted free-base porphyrins: formation, structure and photostability of diprotonated species

Gabriela Dyrda[1] · Rudolf Słota[1] · Małgorzata A. Broda[1] · Giuseppe Mele[2]

Received: 30 April 2015 / Accepted: 25 August 2015 / Published online: 4 September 2015

Abstract Susceptibility to interact with trifluoroacetic acid (TFA) of selected free-base porphyrins, including a novel lipophilic 3-*n*-pentadecyl(phenoxy)-ethoxy-phenyl-substituted porphyrin, and photostability of their diprotonated compounds was explored in benzene and N,N-dimethylformamide (DMF). Results have been discussed in terms of the commonly applied pK_a-based procedure and confronted with a simple approach derived from experimentally-determined correlations reflecting the porphyrins affinity for TFA. Density functional theory (DFT) has proved the porphyrin moiety creates stable diprotonated species involving two TFA molecules, in which the fluorine atoms effectively contribute to the overall interaction of the acid with the porphyrin macrocycle. The relevance of the *meso*-substituent and ambient medium to the reactivity and photostability of diverse porphyrin derivatives was emphasized and referred to structural features of the investigated diprotonated porphyrins.

Keywords Free-base porphyrins · Protonation · Photobleaching · Lipophilic porphyrins · DFT computation

Electronic supplementary material The online version of this article (doi:10.1007/s11164-015-2245-5) contains supplementary material, which is available to authorized users.

✉ Rudolf Słota
rslota@uni.opole.pl

[1] Faculty of Chemistry, Opole University, ul. Oleska 48, 45-052 Opole, Poland

[2] Department of Engineering for Innovation, University of Salento, Via Arnesano, 73100 Lecce, Italy

Introduction

The free-base porphyrins (H_2Por), in contrast to their metallated derivatives, display a different chemical behavior in the presence of electron-acceptor species [1]. The most explored case is the porphyrin's chemistry in the presence of protic species in organic solvents, usually described in terms of acid–base equilibrium [2–5]. The significance of protonated H_2Por species follows from the fact that they may serve as convenient models which can be used to explore the strength and photochemistry of the chromophore in structurally different porphyrin units.

It is generally accepted that, under acidic conditions, the porphyrin core (Fig. 1) undergoes protonation at one or both of the pyrrole nitrogen atoms, which results in formation of either a monocation or dication, respectively [6–18]. Although the existence of the mono-protonated cation was reported elsewhere, the diprotonated porphyrin form was practically the only stable product found in acidic media [9–17]. The dication, H_4Por^{2+}, can be obtained by adding some acid into a solution of H_2Por in an organic solvent. Trifluoroacetic acid (TFA) is a common electron-acceptor reagent, frequently used for this reason. The reaction of porphyrins with TFA and/or other acceptor species (e.g., HCl, BF_3, $SbCl_3$ etc.) in homogenous solutions can be monitored by electronic absorption spectra measurements [19–33].

Theoretical ab initio calculations allowed analyzing the structure and nature of the H_2Por-acceptor adducts. Stability of the modified macrocycle has been related directly to the bonding stress resulting from hosting one or two electron acceptor species at the porphyrin core. In consequence, the symmetry of the initially quasi-flat molecule considerably changes [34–38]. Due to redistribution of electronic density within the bonding system of the core, the newly created adducts may reveal unique chemical and photochemical properties, unlike typical porphyrins, first reflected in their absorption and fluorescence spectra [20].

Diverse tetra-*meso*-aryl-substituted H_2Pors, further formulated as H_2Por–R_4 (where R is a phenol derivative), have been well described in the relevant literature [36]. It was found that electron-donating functional groups may considerably increase the activity of the porphyrin moiety towards protonation and, hence, its chemical stability [37]. This usually has been addressed to the acid/base relation in a porphyrin-protic acid system even in organic solvents, although such approximation is based on a concept dedicated primarily to aqueous solutions (Henderson–Hasselbalch equation). In fact, the porphyrin-acid interaction expressed in terms of acid/base dissociation constants may have raised some objections, mainly because of the unidentified ionization state of the interacting species and the unknown

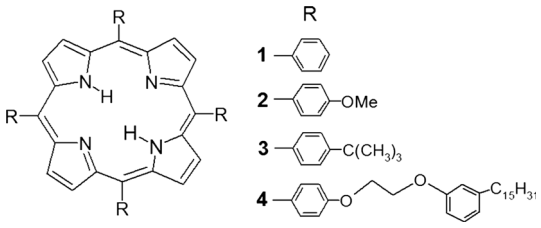

Fig. 1 The *meso*-substituted porphyrin (H_2Por–R_4) and the functional groups (R) involved in compounds used in this study

contribution of the acid-derived anion to the postulated equilibrium states. It must be noted that CF_3COO^- is yet a strong Lewis acid, and its impact upon the condition of the porphyrin system has not been elucidated thus far. Hence, the pK_a or pK_b quantities reported elsewhere are occasionally referred to as "relative acidity constant" [9] and/or "apparent pK_a" [10]. With this in mind, we have demonstrated a simple alternative approach to assess the porphyrin's susceptibility to form a diprotonated chromophore system (*bis*-TFA adduct), based on direct correlation analysis applied to raw experimental data. The proposed method, although not immediately addressed to the protonation mechanism itself, yet may help analysis of protonation data, allowing avoidance of the above mentioned acid–base equilibrium approximation. This may appear particularly useful in estimating the activity of diversely substituted H_2Por derivatives.

Photodegradation of the macrocycle in H_2Por has usually been attributed to oxygen-mediated reactions that may be prompted due to absorption of photonic energy by both the porphyrin substrate and molecular oxygen. Since excited porphyrins may sensitize O_2 species to give rise to the formation of singlet molecular oxygen ($^1\Delta_g$) along with some other radicals, it is frequently referred to as the principal reason for the photo-bleaching of porphyrins [39–42]. Hence, it is important to assess the stability range for the most promising porphyrin systems, including their protonated forms. Moreover, the lack of published experimental data strictly concerning the photostability of diprotonated H_2Por compounds prompted us to report on this issue too.

A novel symmetrically tetra-*meso*-functionalized free-base porphyrin involving 3-*n*-pentadecyl(phenoxy)-ethoxy-phenyl substituents [43] has been presented here for the first time and its activity towards TFA was compared with commonly studied compounds. This new lipophilic porphyrin was partially derived from cardanol oil produced from renewable resources [44]. In addition to the typical optoelectronic properties of porphyrins, this particular derivative has demonstrated excellent solubility both in organic solvents and lipophilic media, as well as very good processability and adhesivity to smooth surfaces. Hence, this compound could possibly be interesting for biological and medical applications, and useful as a (photo)active component in chemo- and bio-sensors.

A density functional theory (DFT) approach dedicated to the interaction of TFA with the porphyrin core in H_2Por allowed demonstrating how far structural modifications may go in diprotonated porphyrin molecules and how this can affect the stability thereof.

Experimental

Extensive spectral and other experimental data have been reported in the Supplementary Information (SI) appendix . Where relevant in the "Results and discussion" section, the appropriate figures referring to the SI material have been numbered in the following way S-1, S-2, etc.

Materials

5,10,15,20-Tetraphenylporphine (**1**) and *5,10,15,20*-tetrakis(4-methoxy-phenyl)porphine (**2**) were purchased from Sigma-Aldrich; *5,10,15,20*-tetra(4-tert-butylphenyl)-porphine (**3**) and *5,10,15,20*-tetrakis-[4-(2-(3-pentadecyl)phenoxy)-ethoxy]phenyl porphyrin (**4**) were obtained according to the methods reported elsewhere [44, 45]. The relevant structures have been shown in Fig. 1. Benzene, N,N-dimethylformamide (DMF) and TFA were provided by Sigma-Aldrich.

Spectrophotometric measurements

A JASCO V-670 spectrophotometer (Spectra Manager V.2 software) and a 1-cm quartz cuvettes were used to measure electronic absorption spectra in the ultraviolet-vible light (UV–Vis) range.

Porphyrin protonation

The porphyrins were investigated in benzene and DMF. This choice mainly followed from extreme different properties featured by these liquids, and, beyond other issues, the results were expected to elucidate how far the nature of the solvent might have affected the plausibility of protonation studies. Benzene is considered much more suitable since it is non-polar and chemically inert under typical conditions used in such tests. DMF, instead, is a polar proton-acceptor compound and its use in a bulk together with TFA may be regarded controversial. However, DMF is effective as a porphyrin solvent and, hence, widely applied, also in protonation experiments [32].

The porphyrins **1**–**4** were all explored in the concentration range of 1.0–5.0 $\times$ 10^{-6} mol/dm^3. A 2-ml sample of the porphyrin solution was treated with 1 ml of TFA of a specified concentration, mixed and its UV–Vis absorption spectrum was measured. This procedure was repeated by gradually increasing the concentration of TFA, until the maximum possible amount of the diprotonated form of the porphyrin was produced. Protonation was assumed complete when the intensity of the newly emerged red-shifted B band (Soret) achieved its maximum (see "The protonation progress" section). The demand for TFA in these titrations clearly depends on the solvent polarity and its "basicity"; hence, it was higher in the case of DMF solutions, compared to benzene. To demonstrate the relation between the molecular structure of the porphyrin and the amount of the acid involved in protonation, the porphyrin solutions were prepared to display similar initial absorbance values (Table 1). Molar absorptivities (ε) are provided in the SI appendix (Table S-1). For the sake of brevity, wherever relevant, the diprotonated porphyrins were all labeled H_4Por^{2+} regardless of the compound type. Experimental results were analyzed by the means of CurveExpert v.1.34 software (a curve-fitting system for Windows Double-precision/32-bit package).

Table 1 Parameters of the protonation process

Compound	**1**	**2**	**3**	**4**
Benzene				
A_o	1.21	1.18	1.19	1.20
A_{max}	1.22	1.15	1.16	1.16
c_{ef}	2.4×10^{-4}	8.5×10^{-5}	1.7×10^{-4}	9.6×10^{-5}
DMF				
A_o	1.22	1.26	1.21	1.24
A_{max}	1.07	0.90	1.03	1.00
c_{ef}	1.55	0.19	0.66	0.29

A_o absorbance of the initial $H_2Por–R_4$ solution; A_{max} maximum absorbance of the H_4Por^{2+} form and the experimentally determined effective concentration of trifluoroacetic acid (TFA), c_{ef} (mol/dm^3); *DMF* N,N-dimethylformamide

Photostability studies

To assess the photostability, a similar procedure was applied, as in our previously reported work [46, 47]. Porphyrin solutions were exposed to UV radiation ($\lambda = 366$ nm) in a quartz cuvette fitted with a Teflon stopper and thermostated at 20 °C; irradiance $I_{UV} = 150$ μW/cm^2 (measured at the wall facing the light source). The explored solutions were not de-aerated prior to testing. Kinetic curves, $A = f(t)$, reflecting the porphyrin decay due to irradiation were determined from time-correlated absorbance measurements, i.e., from the peak value (A) of the B-band (Soret). The effective rate constants, k_e, for the photodegradation process were computed directly from kinetic data (CurveExpert v.1.34 software).

Theoretical calculations

All calculations were performed with the Gaussian 09 software [48] using DFT methods. The B3LYP [49, 50] and M06-2X [51, 52] functionals were used with the 6–31 + G(d) basis set by Pople et al. [53]. The hybrid meta exchange correlation functional M06-2X was chosen since it is recommended for calculations dedicated to non-covalent interactions, and proved very effective in prediction of electronic and geometric structures of porphyrins [54, 55]. Geometry optimization and vibrational analysis of the porphine adduct including two molecules of TFA (and/or acetic acid, HAc, as reference) was carried out in the gas phase without symmetry constraints. All normal frequencies at the optimized geometry are real, showing that it is indeed a stable minimum. The intermolecular interaction energies (ΔE) for H_2Por + 2 TFA (and/or 2 HAc) adducts were calculated using the Boys and Bernardi counterpoise (CP) method to correct the basis set superposition error (BSSE) [56]. Dihedral angles reported in "The acid–base equilibrium" section were calculated using the Mercury 1.3 software (http://www.ccdc.cam.ac.uk/mercury/).

At this stage of investigation, we have demonstrated a simplified DFT approach, only to show the general trend and the possible extent of changes upon addition of a

stoichiometric amount of TFA, i.e., assuming the ratio of the free base to TFA was 1:2. In fact, under real experimental conditions, the liquid phase contained a great excess of TFA added (see p. 3.2). For this reason, such calculations should have involved not only the solvent itself but also the highly possible interactions between the solvent and TFA should be taken into consideration, with all of the possible consequences, which might have resulted from this fact. These issues, however, will be addressed in an advanced theoretical follow-up work.

Results and discussion

The protonation progress

Conversion from the initial purple form, $H_2Por–R_4$, into its yellow–green diprotonated modification was followed from the evolution of electronic absorption spectra measured at different concentrations of TFA. Immediately after addition of the acid into the porphyrin solution, a state of equilibrium was established, which was confirmed by the UV–Vis spectrum showing no further variations in both the position and intensity of the absorption bands. Therefore, one may assume that the TFA-treated porphyrins remain stable at any reaction stage. In all studied cases, including tests performed at very low TFA concentrations, protonation of the porphyrin core produced similar changes in the UV–Vis absorption spectra (Fig. 2a, and Figs. S-1, S-2, S-3), considered typical for this class of compounds [13, 17]. However, it must be emphasized that the amount of TFA necessary to achieve a completely protonated porphyrin system (effective TFA concentration, c_{ef}) has proved to vary with the solvent and the compound explored (Table 1), a fact which is often neglected in reported data. This relation is evident from the graphs shown in Figs. 2b, c, featuring the formation of the diprotonated porphyrin form.

The curves $A = f(c)$ clearly evolve according to a similar fit equation type, as shown by (1)

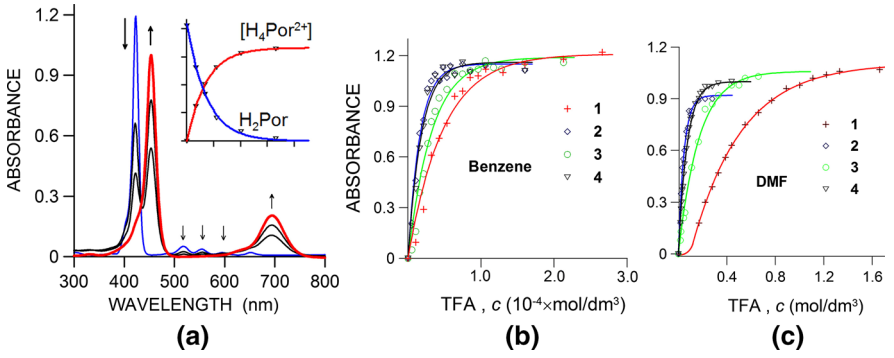

Fig. 2 Effect of TFA on the chromophore system in $H_2Por–R_4$. **a** Formation of the H_4Por^{2+} adduct (diprotonated porphyrin) featured in the UV–Vis spectra of **4** in DMF; *inset* shows the conversion process following the addition of TFA, $A = f(c)$. Evolution of the diprotonated forms of **1**–**4** as a function of TFA concentration (c, mol/dm^3) in benzene (**b**) and DMF (**c**)

$$A = A_{\infty}\left(1 - e^{-\beta c}\right) \quad (1)$$

where A denotes absorbance measured at λ_{max} of the B band and A_{∞} refers to the maximum value achieved for the diprotonated form, c is the TFA concentration in the initial porphyrin solution, and β is the main correlation constant. Some exception was revealed for the compound **1** in DMF, for which a better fit was offered by Eq. (2), as compared with (1)

$$A = a\left(b - e^{-\beta c}\right) \quad (2)$$

where a and b are absorbance-related coefficients (note, that $a \cdot b = A_{\infty}$). This difference apparently results from the fact that in the case of **1**, more acid must be involved during the induction period of the protonation process, in contrast to the other porphyrins.

The equation parameters are collected in Table 2. It should be noted the computed A_{∞} and the experimental A_{max} values (Table 1) were found to be quite similar and the effective amount of TFA (c_{ef}) corresponding to A_{max} in each case goes well with the sequence of the β constant. Incidentally, β may be used to characterize the susceptibility of the porphyrin system to undergo protonation. Large β values mean less acid used in the process and, hence, a more reactive porphyrin core. The highest β is shown by **2** followed by **4**, both of which containing *O*-phenyl components at the *meso* sites, which evidently activate the system, thus making the protonation much easier than with the substituents in **3** and, particularly, the sole phenyl groups in the case of **1**. Similar observations were reported elsewhere [12, 13, 37]. Although the presented approach allows bypass of the acid–base equilibrium treatment discussed below, at this stage, the β coefficient reflecting the "susceptibility to protonation" (affinity for TFA) should be considered in terms of a proposal rather. However, its universal physicochemical significance should be verified soon while studying other systems involving interactions between the porphyrin core and diverse electron acceptor species.

The acid–base equilibrium

The relation between the concentration of system components including the free-base porphyrin and its diprotonated form, as well as an excessive amount of TFA, has usually been described in terms of acid–base equilibrium

Table 2 Parameters of the protonation curves, $A = f(c)$

Compound	**1**	**2**	**3**	**4**
Benzene				
A_{∞}	1.21	1.15	1.19	1.16
β	2.08×10^4	6.11×10^4	3.07×10^4	5.46×10^4
DMF				
A_{∞}	1.40/0.79*	0.92	1.06	1.00
β	2.44	21.7	5.87	13.9

* Refers to *a*/*b* in equation type (2). *DMF* N,N-dimethylformamide

$$H_4Por^{2+} \rightleftarrows 2H^+ + H_2Por \tag{3}$$

and, hence, the equilibrium constant, K_a is given by

$$K_a = \frac{[H^+]^2 \cdot [H_2Por]}{[H_4Por^{2+}]} \tag{4}$$

Following the general approximation of this concept [10], the so-called "observed pK_a constant" can be estimated from a plot of $\log([H_2Por]/[H_4Por^{2+}])$ versus $-\log c$ (where c is the TFA concentration) for the condition $[H_2Por] = [H_4Por^{2+}]$, as presented in Fig. 3. Although dissociation of TFA could not be included into these considerations, it has commonly been assumed to be proportional to the concentration of protons in solution [10, 19]. For the sake of this work, the apparent pK_a constants were determined following the above mentioned procedure, and the results have been shown in Table 3.

As it turned out, the order of magnitude, but also most of the pK_a values, when addressed to the same porphyrin compounds, were similar to those reported elsewhere [5, 10, 18, 37, 57]. Moreover, the sequence of the pK_a values collected in Table 3 appeared convergent with that of the β coefficient assigned to the porphyrin affinity for TFA (Table 2).

As a matter of fact, in all studied cases, the amount of TFA required to achieve the maximum concentration of the H_4Por^{2+} cation considerably exceeded the value following from the assumed adduct composition. For instance, for **1**, the concentration of TFA in benzene was about 20 times greater than the expected value, whereas, in DMF, it was 2×10^5 times more; for **2**, these values were 4 and 5×10^3, respectively. This fact should give some points to consider when discussing any potential equilibrium regarding the H_2Por–TFA system in organic media since these results are indicative of possible intermolecular interactions other than H_2Por–TFA only. The probability of interactions involving bonding of extra TFA molecules by the already-protonated species seems real, as suggested elsewhere [33]. Hence, these additional bonding possibilities may account for the higher demand of TFA observed during the protonation process.

In particular, the great excess of TFA required in DMF compared to benzene may suggest that DMF is not an appropriate solvent in such studies. Hence, the results reported for the tests performed in DMF should be carefully treated. Interestingly, despite the completely different physicochemical character of the solvents used, the course of the protonation process in the both media looks similar. Nevertheless, this

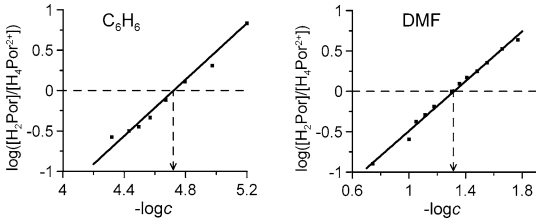

Fig. 3 Determination of pK_a for compound **4** according to [10]; c—concentration of TFA, mol/dm^3

Table 3 Values of pK_a estimated according to [10]

Compound	**1**	**2**	**3**	**4**
Benzene	4.35	4.99	4.44	4.72
DMF	0.32	1.45	0.89	1.31

DMF N,N-dimethylformamide

issue seems not quite clear and needs a plausible explanation. Thus far, protonation of H_2Por in DMF has been reported very occasionally [37] and recently for N-confused porphyrin series [32].

Effect of protonation on the electronic absorption spectra

Another interesting issue revealed in the UV–Vis spectra was the size of the red-shift of absorption bands due to protonation. Distribution of the B and Q bands apparently depends on the kind of the functional group attached at the *meso* site of the macrocycle and, to some extent, on the solvent. The range of λ_{max} values (Δ) for both the *B* and *Q* bands in the spectra of initial forms of the studied porphyrins equals 4–5 nm (the band positions are nearly the same), whereas it becomes much larger after protonation, 13–14 and 29–37 nm for the *B* and *Q* bands, respectively (Table 4; Fig. 4). Such behavior is well known from the literature [37], and usually related to the solvent's polarity [20]. Nevertheless, it is worth highlighting the peculiar flexibility of the molecular system in diverse porphyrin compounds as reflected by these spectral changes, which has been particularly emphasized in Fig. 4, and also reported elsewhere [8].

Table 4 Peak position (λ_{max}, nm) of the B (Soret) and Q bands in the UV–Vis spectra of H_2Por–R_4 and the diprotonated derivatives (H_4Por^{2+}) in benzene and DMF

Compound	**1**	**2**	**3**	**4**	**Δ**
Benzene					
H_2Por–R_4					
B	419	423	421	423	4
Q	514, 547, 589, 647	518, 554, 594, 652	516, 551, 593, 649	518, 554, 594, 652	4–5
(H_4Por^{2+})					
B	438	451	444	451	13
Q	655	684	669	684	29
DMF					
H_2Por–R_4					
B	416	421	419	421	5
Q	513, 546, 589, 645	517, 554, 593, 650	517, 552, 593, 650	517, 555, 594, 649	4–5
(H_4Por^{2+})					
B	439	453	445	453	14
Q	657	694	670	693	37

Δ represents the λ_{max} range (nm); *DMF* N,N-dimethylformamide

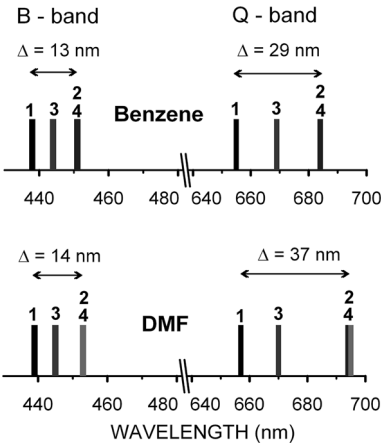

Fig. 4 Distribution of the *B* and *Q* bands in the UV–Vis spectra of diprotonated porphyrins **1**–**4**; the Δ range in λ_{max} reflects the effect of protonation with respect to the compound and solvent used; numbers above the peaks refer to the appropriate porphyrins

In particular, the position of the *Q* bands proved sensitive to protonation. The most red-shifted peaks notably featured the species **2** and **4** either containing four *O*-phenyl units directly anchored at the porphyrin's chromophore system. Such coupling is supposed to activate the porphyrin core by increasing the electronic density within to a definitely larger extent than in the case of **1** and/or **3**. Consequently, this should result i.a. in different distribution of absorption bands in the spectra of protonated porphyrins **1**–**4**, as showed in Fig. 4, indicating the relevance of the *meso*-substituent's nature. Similar conclusions follow from a variety of detailed analyses available elsewhere [13, 19, 37].

One may also note, e.g., from Fig. 2a, that the newly created diprotonated chromophore displays higher symmetry in electronic density distribution with respect to the initial H_2Por compound, despite the porphyrin macrocycle no longer being planar after having combined two additional protons supplied by TFA (see Fig. 5).

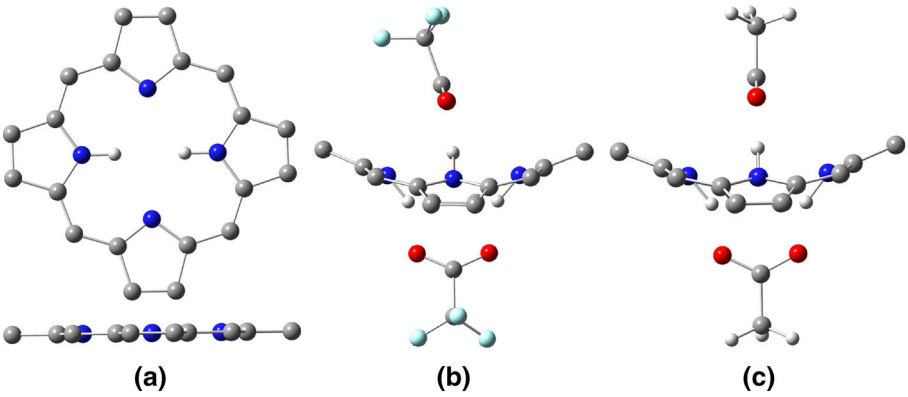

Fig. 5 Deformation of the protonated chromophore (porphyrin core) in a model porphine moiety as revealed in a DFT approach (only the pyrrole-combined protons have been included for brevity); **a** general and side-view of the free-base macrocycle; **b** TFA adduct; **c** HAc adduct

Structural consequences of porphyrin core diprotonation (a DFT approach)

The simple molecular model using a *porphine* moiety (Fig. 5) appeared sufficient to illustrate not only the possible modification of the chromophore system but also supplied useful hints concerning the very probable interaction of the CF_3–COO^- anion with the porphyrin macrocycle. DFT computations performed using the B3LYP and M06-2X functionals provided similar structural results, although energy of the porphyrin-TFA interaction was found about 10 % lower in the first case. However, the results reported in Table 5 refer only to the M06-2X functional, which has been particularly recommended in porphyrin structural calculations [54, 55].

Formation of the H_2Por–$(TFA)_2$ adduct considerably affected the molecular symmetry of the porphyrin moiety. Accommodation of two additional protons resulted in a saddle structure of the set-up, the hydrogen atoms sticking upwards and downwards, and the core plane pointing directly at the oxygen atoms of both TFA species (Fig. 5). The estimated interaction energy appeared rather high; ca. 270 kJ/mol referred to a single H···O bond. The perimeter of the protonated core (S_c) was found only slightly expanded (0.26 %), whereas the mean N–H bond length increased by 3.6 %, compared to the free-base H_2Por molecule. This would mean that all the internal protons were equally strongly combined with the pyrrole units and there was a large contribution of electrostatic forces to the overall bonding energy within the $(H_4Por^{2+})\cdots(OOC–CF_3)_2$ system. Interestingly, the TFA molecules were not found perpendicular to the virtual plane of the porphyrin moiety, unlike the case of the HAc reference. Each of the both TFA anions showed an equal inclination of 70.7° towards the pyrrole ring not involved in the H···O bonding, which would suggest the fluorine atoms effectively participate in the interactions between H_2Por and TFA. Undoubtedly, such interactions would add to the bonding energy of the H_2Por-$(TFA)_2$ adduct, which had proved to be 100 kJ/mol greater in comparison with the effect brought up by acetic acid in H_2Por–$(HAc)_2$.

Diverse activity displayed by different *meso*-aryl-substituted porphyrins has usually been related to the torsion of the *meso*-phenyl rings relative to the virtual macrocycle plane. In fact, the π-electronic systems of the phenyl and the porphyrin core are significantly non-co-planar (Fig. 6; Table 6). A general trend was observed that when the rotation of the phenyl rings had led towards a more flat arrangement, the H_2Por moiety usually revealed higher activity and was found more susceptible to protonation, especially when the phenyl rings were para-functionalized by

Table 5 Selected molecular data (M06-2X) for the base model porphine (H_2Por) and its TFA and HAc adducts: ΔE intermolecular interaction energy; S_c core perimeter (Å), N–H and H–O are the respective mean bond lengths (Å)

Compound	ΔE (kJ/mol)	S_c	N–H	H–O
H_2Por	–	22.048	1.017 (0)	–
H_2Por-$(TFA)_2$	1090	22.105	1.054 (8×10^{-5})	1.651 (1×10^{-3})
H_2Por-$(HAc)_2$	990	22.085	1.084 (2×10^{-3})	1.537 (6×10^{-3})

Standard deviation (SD) is given in parentheses

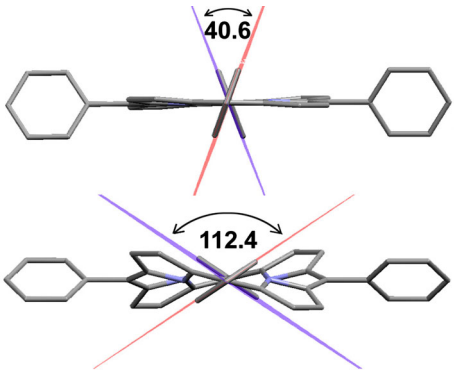

Fig. 6 The dihedral angle (°) between the *trans*-positioned *meso*-aryl rings representing the relative torsion of the benzene rings versus the virtual macrocycle plane in free-base (*top*) and diprotonated (*bottom*) compound **1**

Table 6 Selected DFT structural data for the free-base porphyrins, H_2Por, and their diprotonated forms, (H_4Por^{2+}); dihedral angle (°) between the *trans*-positioned *meso*-aryl rings

Compound	**1**	**2**	**3**	**4**
H_2Por	40.6	48.3	42.0	54.6
(H_4Por^{2+})	112.4	123.9	117.6	126.4

electron-donating groups [19, 37]. Such inductive effect, although less pronounced, was also demonstrated in porphyrins which were *meso*-substituted by only phenyl and alkylo-phenyl groups being almost perpendicular to the macrocycle, as confirmed by theoretical (DFT) studies [8].

Our DFT-based results (Table 6) are convergent with these suggestions. Since the analyzed systems proved sufficiently symmetrical, the magnitude of the phenyl rings rotation was demonstrated by the dihedral angles formed by the *trans*-located phenyls, as defined in Fig. 6 (see also SI Figs. S-4, S-5). In diprotonated species, this angle was found to be considerably increased, mainly due to structural deformation of the macrocycle, which allowed a more free torsion of the quoted phenyls. In particular, compounds **2** and **4** including *O*-phenyl units displayed enhanced rotation of the *meso*-benzene rings towards a more flat arrangement, compared to **3** and **1**. Consequently, the data presented in Table 6 fit well to the sequence of the β coefficient (Table 2) and the distribution of absorption bands reported in Fig. 4.

Photostability studies

Photodegradation of the studied compounds was accompanied by typical spectral changes, as shown in Fig. 7a. Kinetic curves featuring the decay of the photolyzed porphyrins [$A = f(t)$] all followed the simple first-order exponential relation (5), where $A_0 = A(t = 0)$,

$$A = A_0 e^{-k_e t} \tag{5}$$

and demonstrated similar performance on the time scale, as in the example featuring compound **4** shown in Fig. 7b. The effective photolysis rate constant, k_e, can be

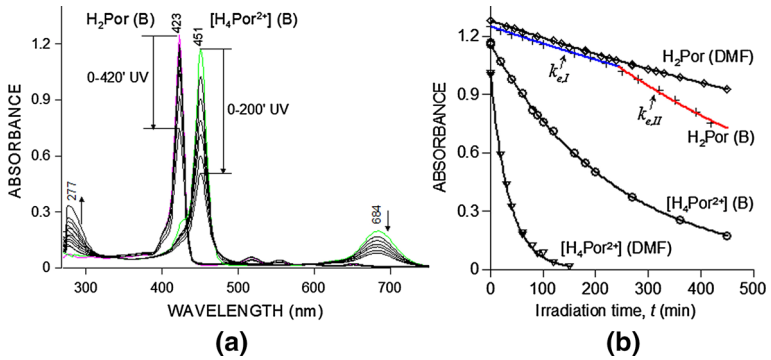

Fig. 7 Photodegradation of the base and diprotonated forms of compound **4** displayed by **a** spectral changes and **b** kinetic curves $A = f(t)$; note the change in kinetics ($k_{e,I} \rightarrow k_{e,II}$) revealed by the free-base H_2Por–R_4 in benzene (B) after 240 min of irradiation; initial concentration of **4** in both benzene and DMF was 4.3×10^{-6} mol/dm^3

used to characterize the compound's photostability and the experimentally determined values are reported in Table 7 (For more experimental data see SI, Figs. S-6–S-11).

Assuming photodegradation is an oxygen-mediated process involving the UV-excited porphyrin moiety, as proved elsewhere [39], its kinetics and effectiveness must be referred to the activity of the chromophore bonding system. As one may learn from Fig. 7 and Table 7, the free-base porphyrins reveal two-step kinetics when exposed to UV light in benzene solution. Initially, the photolysis rate is similar to that in DMF. This fact suggests the time of the reactivity of the chromophore setup has increased, probably due to interaction with some reactive molecules formed during UV-irradiation, such as diverse reactive oxygen species (ROS) and/or formation of less stable intermediates, as follows from some other studies [39, 58]. This effect proved most pronounced for **2**, **4** and **3**, which were found to be also much more susceptible to protonation than compound **1**. The same trend was demonstrated in DMF, thus confirming the important relation between the activity of the porphyrin core and its photostability. The smaller k_e values found for

Table 7 Photolysis effective rate constants, k_e ($10^{-4} \times \text{min}^{-1}$); $I_{UV} = 150$ μW/cm^2; for the free-base porphyrins (H_2Por–R_4) in benzene $k_{e,I}$ and $k_{e,II}$ have been shown ($k_{e,I}/k_{e,II}$); all fitting curves used in order to calculate k_e showed a correlation coefficient $R^2 \geq 0.99$

Compound	**1**	**2**	**3**	**4**
Benzene				
H_2Pp–R_4	2.6/6.9	7.7/19	5.2/17	7.4/18
(H_4Pp^{2+})	82	35	24	42
DMF				
H_2Pp–R_4	3.8	7.1	5.1	7.2
(H_4Pp^{2+})	320	270	320	270

$H_2Por–R_4$ in DMF may definitely be assigned to the partial solvent photolysis, the products thereof could have limited the effect of ROS, at least.

Once protonated, the symmetry of the porphyrin core is changed (Fig. 5) and in consequence the whole molecular system becomes less stable. Furthermore, the polarizing effect induced by the four positively charged pyrrole-linked protons also contributes to the weakening of the bonding setup. However, depending on the electron density delocalized over the chromophore, fixation of two additional protons may have a different impact on the eventual photostability of a diprotonated porphyrin macrocycle. Therefore, compounds **2** and **4** with presumably increased core-electron density (due to coupling with *O*-phenyl groups) may still retain the potential of a relatively more stable bonding within the porphyrin core, than in the case of **1**. On the other hand, the considerably lower photostability of diprotonated compounds in DMF (Table 7) must be related to the much greater amounts of TFA which had to be used to achieve the maximum level of protonation (Table 1). Evidently, acidic conditions are not favorable to the stability of free-base porphyrins when exposed to UV radiation.

Conclusions

Affinity to TFA of a free-base porphyrin compound effectively depends on the type of the *meso* substituent. The general trends observed in benzene and DMF solutions are similar, although these solvents featured different polarity and chemistry. Interaction of the porphyrin moiety with TFA leads to a relatively stable $[H_4Por^{2+}]–(TFA)_2$ adduct, unless exposed to UV radiation. The susceptibility of the chromophore system to accommodate extra protons may be characterized by the β factor, resulting from an exponential correlation determined for the process of porphyrin titration by TFA. This finding has a broader relevance and it may prove crucial to estimating the reactivity (and stability) of diverse porphyrin derivatives, particularly when in contact with small-sized electron-acceptor species.

Finally, it must be emphasized, that this investigation has a wider context with respect to the activity of porphyrins in catalytic and biological systems, in which the interactions with diverse electron-acceptor species are considered of fundamental importance. A comprehensive knowledge concerning the photostability of pre-activated (e.g., protonated) porphyrin-based materials is essential to assess their applicability i.a. as photosensitizers in medical therapies like photodynamic therapy (PDT) and/or state-of-the-art photocatalysts and chemosensors.

Acknowledgments Calculations were carried out at the Wrocław Centre for Networking and Supercomputing (http://www.wcss.wroc.pl), and at the Academic Computer Centre Cyfronet, AGH, Kraków, Grant MNiI/SGI2800/UOpolski/059/2004.

References

1. C. Wang, C.C. Wamser, J. Phys. Chem. A **118**, 3605 (2014)
2. B.M. Harvey, P.E. Hoggard, Monatsh. Chem. **143**, 1101 (2012)
3. Y.B. Ivanova, N.V. Chizhova, Russ. J. Gen. Chem. **83**, 124 (2013)
4. T.P.G. Sutter, R. Rahim, P. Hambright, J.C. Bommer, M. Kumar, P. Neta, J. Chem. Soc., Faraday Trans. **89**, 495 (1993)
5. Y. Fang, P. Bhyrappa, Z. Ou, K.M. Kadish, Chem. Eur. J. **20**, 524 (2014)
6. T. Honda, T. Kojima, S. Fukuzumi, Chem. Commun. **33**, 4994 (2009)
7. B. Cheng, Q.O. Munro, H.M. Marques, W.R. Scheidt, J. Am. Chem. Soc. **119**, 10732 (1997)
8. M. Presselt, W. Dehaen, W. Maes, A. Klamt, T. Martıinez, W.J.D. Beenken, M. Kruk, Phys. Chem. Chem. Phys. **17**, 14096 (2015)
9. M.J. Webb, N. Bampos, Chem. Science. **3**, 2351 (2012)
10. P.K. Goldberg, T.J. Pundsack, K.E. Splan, J. Phys. Chem. A **115**, 10452 (2011)
11. S. Zakavi, R. Omidyan, L. Ebrahimi, F. Heidarizadi, Inorg. Chem. Commun. **14**, 1827 (2011)
12. S. Zakavi, N.G. Gharab, Polyhedron **26**, 2425 (2007)
13. J.R. Weinkauf, S.W. Cooper, A. Schweiger, C.C. Wamser, J. Phys. Chem. A **107**, 3486 (2003)
14. A. Rosa, G. Ricciardim, E. Baerends, J. Phys. Chem. A **107**, 11468 (2003)
15. G. de Luca, A. Romeo, L.M. Scolaro, J. Phys. Chem. B **110**, 14135 (2006)
16. G. de Luca, A. Romeo, L.M. Scolaro, J. Phys. Chem. B **109**, 7149 (2005)
17. D.L. Akins, H.R. Zhu, C.H. Guo, J. Phys. Chem. **100**, 5420 (1996)
18. A.B. Rudine, B.D. del Fatti, C.C. Wamser, J. Org. Chem. **78**, 6040 (2013)
19. M.M. Kruk, A.S. Starukhin, W. Maes, Macroheterocycles **4**, 69 (2011)
20. G. de Luca, A. Romeo, L.M. Scolaro, G. Ricciardi, A. Rosa, Inorg. Chem. **46**, 5979 (2007)
21. A.S. Sadjadi, R.I. Walter, J.S. Harwood, J. Phys. Chem. A **101**, 9948 (1997)
22. S. Thyagarajan, T. Leiding, S. Peterson-Årsköld, A.V. Cheprakov, S.A. Vinogradov, Inorg. Chem. **49**, 9909 (2010)
23. S. Juillard, Y. Ferrand, G. Simonneaux, L. Toupet, Tetrahedron **61**, 3489 (2005)
24. D. Mohajer, S. Zakavi, S. Rayati, M. Zahedi, N. Safari, H.R. Khavasi, S. Shahbazian, New J. Chem. **28**, 1600 (2004)
25. M. Asadi, A. Zabardasti, V. Karimivand, J. Ghasemi, Polyhedron **21**, 1255 (2002)
26. M. Asadi, A. Zabardasti, J. Ghasemi, Polyhedron **21**, 683 (2002)
27. H. Molaei, H. Dehghani, Inorg. Chim. Act. **384**, 133 (2012)
28. S. Aronoff, J. Am. Soc. **62**, 428 (1958)
29. H. Dehghani, A.R.A. Sardrood, Polyhedron **26**, 4263 (2007)
30. S. Zakavi, H. Rahiminezhad, R. Alizadeh, Spectrochim. Act. Part A **77**, 994 (2010)
31. D. Mohajer, E. Sakhtemanian, S. Rayati, S. Zakavi, Spectrochim. Act. Part A **69**, 998 (2008)
32. Z. Ou, X. Chen, L. Ye, S. Xue, Y. Fang, X. Jiang, K.M. Kadish, J. Porphyr. Phthalocyanines **19**, 251 (2015)
33. M.O. Senge, Z. Naturforsch. **55 b**, 336 (2000)
34. L. Moroni, C. Gellini, P.R. Salvi, Macrocycles J. Phys. Chem. A **112**, 11044 (2008)
35. A. Marcelli, P. Foggi, L. Moroni, C. Gellini, P.R. Salvi, I.J. Badovinac, J. Phys. Chem. A **111**, 2276 (2007)
36. J.A.S. Cavaleiro, A.C. Tomé, M.G.P.M.S. Neves, in *Handbook of Porphyrin Science*, ed. by K.M. Kadish, K.M. Smith, R. Guilard, (World Scientific Publishing Co., Singapore, 2, 2010), p. 193
37. M. Meot-Ner, A.D. Adler, J. Am. Chem. Soc. **97**, 5107 (1975)
38. T. Bruhn, C.H. Bruckner, Phys. Chem. Chem. Phys. **17**, 356 (2015)
39. J.A.S. Cavaleiro, G.P.M.S. Neves, M.J.E. Hewlins, A.H. Jackson, J. Chem. Soc. Perkin Trans. **1**, 1937–1943 (1990)
40. J.A.S. Cavaleiro, H. Görner, P.S.S. Lacerda, J.G. MacDonald, G. Mark, R.S. Nohr, G.P.M.S. Neves, H.P. Schuchmannb, C. von Sonntag, A.C. Tomé, J. Photochem. Photobiol. A Chem. **144**, 131 (2001)
41. J. Ferreira, P.F.C. Menezes, C. Kurachi, C.H. Sibata, R.R. Allison, V.S. Bagnato, Las. Phys. Lett. **4**, 743 (2007)
42. M.S. Silva, G.P.M.S. Neves, R.L. Martins, J.A.S. Cavaleiro, T. Boschi, P. Tagliatesta, J. Porphyr. Phthalocyanines **2**, 45 (1998)
43. O.A. Attanasi, R. del Sole, P. Filippone, S.E. Mazzetto, G. Mele, G. Vasapollo, J. Porphyr. Phthalocyanines **8**, 1276 (2004)

44. G. Mele, G. Vasapollo, Org. Chem. **5**, 243 (2008)
45. G. Mele, R. del Sole, G. Vasapollo, E. García-López, L. Palmisano, M. Schiavello, J. Catal. **217**, 334 (2003)
46. R. Słota, G. Dyrda, Inorg. Chem. **42**, 5743 (2003)
47. R. Słota, G. Dyrda, M. Hofer, G. Mele, E. Bloise, R. del Sole, Molecules **17**, 10738 (2012)
48. Gaussian 09, Revision D.01, M. J. Frisch, G. W. Trucks, H. B. Schlegel, G. E. Scuseria, M. A. Robb, J. R. Cheeseman, G. Scalmani, V. Barone, B. Mennucci, G. A. Petersson, H. Nakatsuji, M. Caricato, X. Li, H. P. Hratchian, A. F. Izmaylov, J. Bloino, G. Zheng, J. L. Sonnenberg, M. Hada, M. Ehara, K. Toyota, R. Fukuda, J. Hasegawa, M. Ishida, T. Nakajima, Y. Honda, O. Kitao, H. Nakai, T. Vreven, J. A. Montgomery, Jr., J. E. Peralta, F. Ogliaro, M. Bearpark, J. J. Heyd, E. Brothers, K. N. Kudin, V. N. Staroverov, R. Kobayashi, J. Normand, K. Raghavachari, A. Rendell, J. C. Burant, S. S. Iyengar, J. Tomasi, M. Cossi, N. Rega, J. M. Millam, M. Klene, J. E. Knox, J. B. Cross, V. Bakken, C. Adamo, J. Jaramillo, R. Gomperts, R. E. Stratmann, O. Yazyev, A. J. Austin, R. Cammi, C. Pomelli, J. W. Ochterski, R. L. Martin, K. Morokuma, V. G. Zakrzewski, G. A. Voth, P. Salvador, J. J. Dannenberg, S. Dapprich, A. D. Daniels, Ö. Farkas, J. B. Foresman, J. V. Ortiz, J. Cioslowski, D. J. Fox, Gaussian, Inc. (Wallingford CT, 2009)
49. A.D. Becke, J. Chem. Phys. **98**, 1372 (1993)
50. C. Lee, W. Yang, R.G. Parr, Phys. Rev. B **37**, 785 (1998)
51. Y. Zhao, D.G. Truhlar, Theor. Chem. Acc. **120**, 215 (2008)
52. Y. Zhao, D.G. Truhlar, Acc. Chem. Res. **41**, 157 (2008)
53. R. Ditchfield, W.J. Hehre, J.A. Pople, J. Chem. Phys. **54**, 720 (1971)
54. M.J. Lee, M.P. Balanay, D.H. Kim, Theor. Chem. Acc. **131**, 1 (2012)
55. D. Tzeli, I.D. Petsalakis, G. Theodorakopoulos, J. Phys. Chem. A **115**, 11749 (2011)
56. S.F. Boys, F. Bernardi, Mol. Phys. **19**, 553 (1970)
57. A.A. Starikova, A.B. Valiotti, A.A. Pendin, Russ. J. Gen. Chem. **84**, 98 (2014)
58. R. Bonnett, G. Martinez, Tetrahedron **57**, 9513 (2001)